Meccanica (2025) 60:3353–3363
https://doi.org/10.1007/s11012-025-01999-z

RESEARCH

Application of stabilized contaminated soils as metaconcrete aggregates

Antonella Petrillo · Giuseppina Di Chiara · Annamaria Acampora · Fernando Fraternali · Ilenia Farina

Received: 1 April 2025 / Accepted: 7 May 2025 / Published online: 28 May 2025
© The Author(s) 2025, corrected publication 2025

Abstract We present an initial study on the use of contaminated soils, effectively treated through a solidification and stabilization (S/S) process that renders them inert, as encapsulated aggregates in the creation of novel metaconcretes. Several mix designs of solidified and stabilized soils are carefully examined, and their physical and mechanical properties are characterized experimentally. These properties are crucial for determining how these treated soils can be effectively incorporated into metaconcretes, a class of materials known for their unique ability to attenuate mechanical waves through resonant structures. The frequency bandgap response of metaconcretes incorporating rubber-coated aggregates made from solidified soils is studied using analytical formulations. The results indicate that the proposed reutilization technique for contaminated soils not only ensures their safety but also offers significant potential for applications in the construction of blast-protective structures and seismic-shielding metamaterials.

Keywords Stabilization · Solidification · Contaminated soils · Metaconcrete

All authors have contributred equally to this work.

A. Petrillo · A. Acampora · I. Farina
Department of Engineering, University of Naples "Parthenope", Naples, Italy
e-mail: antonella.petrillo@uniparthenope.it

A. Acampora
e-mail: annamaria.acampora001@studenti.uniparthenope.it

I. Farina
e-mail: ilenia.farina@uniparthenope.it

G. Di Chiara · F. Fraternali (✉)
Department of Civil Engineering, University of Salerno, Fisciano, Italy
e-mail: f.fraternali@unisa.it

G. Di Chiara
e-mail: gdichiara@unisa.it

G. Di Chiara
Department of Civil Engineering and Architecture, University of Catania, Catania, Italy

1 Introduction

Numerous studies in the literature have demonstrated that the stabilization and solidification (S/S) process is highly effective in remediating contaminated soils (see, for example, [1] and references therein). Stabilization, also known as the immobilization phase of contaminants, combined with solidification, which encapsulates contaminants within a solid matrix, significantly reduces environmental and human health risks. In the early applications of this technique, Portland cement was the primary binding agent used as the solid matrix [2]. However, advancements in the stabilization process have led to the incorporation of alternative materials, such as pozzolanic compounds, fly ash [3], rice husk ash [4],

ground granulated blast furnace slag (GGBS) [5], and bentonite [6]. These additions have enhanced the efficiency and versatility of the process, allowing it to be applied to a broader range of contaminated sites. The partial substitution of Portland cement with alternative materials that have lower energy content and carbon footprints significantly reduces the material's embedded carbon. These materials, often by-products of industrial processes like fly ash (FA) and ground granulated blast furnace slag (GGBFS), offer an eco-friendly alternative. Their use in contaminated soil stabilization minimizes reliance on Portland cement while efficiently managing industrial waste, improving sustainability [7].

FA, a coal combustion by-product, enhances mechanical strength and reduces porosity due to its pozzolanic properties, forming calcium silicate hydrates when reacting with calcium hydroxide [8]. It also binds with contaminants, reducing their mobility and preventing environmental spread. GGBFS, with its hydraulic properties, improves resistance to expansion, contraction, and sulfate-induced corrosion critical in hazardous soil stabilization [9–13]. The combined use of FA and GGBFS lowers cement demand, cutting CO_2 emissions and enhancing ecological sustainability [14]. This approach not only strengthens mechanical properties and durability but also promotes sustainable stabilization techniques, repurposing industrial by-products for environmental remediation and engineering applications [15]. A critical aspect of S/S treatment is the proper characterization of contaminated soil, which includes analyzing contaminant type, concentration, pH, and leaching behavior. The S/S technique has demonstrated remarkable effectiveness in treating a wide variety of hazardous waste, including inorganic, organic, and mixed contaminants [16]. It has also been successfully applied to the remediation of marine sediments [17, 18], which pose additional environmental challenges due to their complex composition and potential for contaminant migration. Long-term studies further confirm the reliability of this approach. For instance, findings by [19] indicate that even 17 years after treatment, stabilized soil continues to meet performance criteria, underscoring S/S as a robust and durable remediation strategy. At the conclusion of the process, the treated soil is structurally stable, non-hazardous, and environmentally safe, as the encapsulation mechanism effectively prevents pollutant release into the surrounding environment.

Over the past decade, metaconcretes have emerged as a new class of concrete materials incorporating engineered aggregates with metamaterial properties [20, 21]. A research group led by Anna Pandolfi and Michael Ortiz first explored combining local resonant metamaterials (LRM) with cement to create materials resilient to extreme loads like explosions [20]. This led to the development of metaconcrete, which is characterized by an external soft coating encapsulating a heavy spherical core (the resonator) instead of conventional gravel. Internal resonators dissipate energy when the dynamic load frequency matches that of the aggregates, creating frequency bandgaps where mechanical waves cannot propagate due to a negative mass effect [21]. Mitchell et al. later quantified resonant behavior within aggregates using the transmission coefficient to measure wave energy absorption [22]. Since 2017, experiments on metaconcrete's ability to mitigate explosive loading have yielded promising results. Non-destructive dynamic tests have shown a significant reduction in transmitted signal amplitude compared to conventional concrete, depending on the type of inclusions and material properties [23, 26]. Building on this research, Chen et al. [27] developed an analytical predictive formula for local resonant bandgap generation, linking bandgap initiation to the resonator's translational vibration mode and the cutoff frequency to the resonator-matrix coupling strength. Xu et al. [28] expanded this study using finite element simulations to analyze bandgap regions, demonstrating how core size, coating thickness, and core density influence attenuation performance. They also proposed a flowchart for designing metaconcretes with multiple resonance frequencies. A 2024 study introduced rubber aggregates with shielding functionality to enhance metaconcrete's resistance, analyzing mesoscale wave attenuation and performance regulation [29]. The effects of aggregate shape on the bandgap properties of metaconcretes have been studied in [30]. Different mechanical nacre-like metamaterials, featuring a brick-and-mortar architecture and potential applications in civil engineering, have been proposed in in [31, 32].

This study explores the potential use of contaminated soils, which are effectively treated through a stabilization/solidification (S/S) process, as encapsulated aggregates in the creation of novel metaconcretes. The S/S process involves treating contaminated soils to render them inert and stable, effectively

eliminating the environmental hazards they may present. The final product of this process is a safe material that no longer poses a risk to human health or the environment. By encapsulating this stabilized material within a soft coating, which is then surrounded by a cementitious matrix, the contaminated soil can be safely integrated into a composite material without direct exposure to the surrounding environment. This encapsulation approach could lead to the development of a new type of metaconcrete, a material that combines the advantages of waste reuse with advanced engineering properties. This novel material, which we will refer to as StabSoil MetaConcrete (SSMC), represents an innovative way to repurpose contaminated soils, turning them into functional components of construction materials. The resulting SSMC material offers the potential to enhance the performance of traditional concrete, particularly in applications requiring improved wave attenuation, such as, e.g., in blast protection structures and meta-foundations of earthquake proof buildings [20]. We begin by investigating the physical and mechanical properties of various mix designs of contaminated soils that have been treated through the stabilization/solidification (S/S) process (Sect. 2). This section lays the foundation for understanding how different soil treatments affect the overall material properties, which are crucial for determining their suitability as components of metaconcrete. Sect. 3 provides a brief overview of the analytical formulation used to predict the bandgap response of metaconcretes, as presented in [27]. This formulation serves as the basis for the parametric study conducted in Sect. 4, where we analyze the bandgap response of different StabSoil MetaConcrete (SSMC) configurations. Finally, Sect. 5 offers concluding remarks and outlines potential directions for future research, emphasizing opportunities for further optimizing and applying SSMC in various engineering applications.

2 Physical properties of stabilized contaminated soils used

2.1 Material selection

Contaminated soils from industrial sites in the province of Naples were collected using excavators and analyzed in this study. The samples exhibit characteristics indicative of significant contamination by heavy metals and organic chemical compounds. This soil, subjected to various chemical and leaching analyses, shows values that, in some cases, exceed regulatory limits, highlighting the need for continuous monitoring and potential remediation measures. Chemically, the soil sample contains significant concentrations of heavy metals, particularly arsenic (72.0 mg/kg), cadmium (2.4 mg/kg), lead (37.3 mg/kg), and mercury (2.2 mg/kg). These metals are key indicators of pollution, often stemming from industrial activities, and can severely impact soil quality and ecosystem health. Additionally, the presence of nickel (28.9 mg/kg) and cobalt (6.0 mg/kg) further confirms heavy metal contamination, while zinc (25.4 mg/kg) is also relevant concerning legal thresholds. Of particular concern is the contamination from hexavalent chromium (28.9 mg/kg), a highly toxic and carcinogenic compound. Aromatic organic compounds, including benzene, ethylbenzene, toluene, and xylene, are present at levels below legal limits but still warrant attention. Chlorinated aliphatic compounds and non-carcinogenic chlorinated compounds are also detected. Although their concentrations comply with established limits, they should not be disregarded in an environmental monitoring context. Leaching tests were conducted following the UNI EN 12457–2 method. The soil sample exhibited concerning values for several chemical substances, as detailed in Table 1.

The results indicate that the soil sample exhibits significant contaminant mobility, with substances such as arsenic (0.12 mg/L), cadmium (0.02 mg/L), and lead (0.6 mg/L) capable of easily percolating into the subsurface and groundwater, increasing the risk of local water resource contamination. The presence of fluoride (1.05 mg/L) and sulfate (210 mg/L) in the leaching tests suggests a potential impact on water quality, while elevated chloride levels (420 mg/L) may indicate contamination from soluble salts associated with industrial activities. The zinc concentration (4.0 mg/L) is also notable, exceeding regulatory limits in some cases. Overall, the data suggests that proper soil management is necessary, with continuous monitoring of both soil and groundwater quality. Remediation measures should be prioritized, particularly for the most hazardous substances, such as arsenic, cadmium, and mercury (0.03 mg/L). Additionally, the long-term effectiveness of implemented solutions should be regularly assessed.

Table 1 Leaching test results: key contaminants in the examined soil

Contaminant	Result	UM	Limits (Ref.1)	Limits (Ref.2)	Limits (Ref.3)
Arsenic	0.12	mg/L	0.2	2.5	0.05
Cadmium	0.02	mg/L	0.1	0.5	0.005
Lead	0.6	mg/L	1	5	0.05
Total chromium	0.8	mg/L	1	7	0.05
Mercury	0.03	mg/L	0.02	0.2	0.001
Zinc	4	mg/L	5	20	3
Fluorides	1.05	mg/L	15	50	1.5
Sulfates	210	mg/L	5000	5000	250

In this context, stabilization techniques were investigated to mitigate the mobility of contaminants. The stabilization materials used in this study included fly ash (FA), ground granulated blast furnace slag (GGBFS), and Portland cement (Table 2).

Specifically, fly ash from municipal solid waste incineration (MSWI-FA) was considered. Prior to use, the MSWI-FA underwent a washing treatment (W-FA) to reduce its chloride and sulfate content. For this process, 5 kg of MSWI-FA was washed with deionized water in a continuous stirred tank reactor (CSTR). The pretreatment was conducted with a liquid-to-solid (L/S) ratio of 2.5 and a retention time of 3 h per phase. After pretreatment, the W-FA was collected by filtration and dried at 45 °C. All stabilization materials were subjected to detailed chemical and physical characterization using various advanced analytical techniques.

Energy dispersive spectroscopy (EDS), X-ray diffraction (XRD), scanning electron microscopy (SEM), thermogravimetric analysis (TGA), and particle size distribution analysis were performed. The results, presented in Table 2, indicate that MSWI-FA predominantly consists of calcium oxides (CaO), sodium chloride (NaCl), and calcium sulfate ($CaSO_4$), imparting properties suitable for pozzolanic reactivity. EDS analysis revealed significant amounts of iron oxides, silica, and alumina in MSWI-FA, which, together with calcium, facilitated the formation of cementitious bonds during the solidification process. Regarding GGBFS, it was primarily composed of silicon, calcium, iron, and magnesium oxides, with an amorphous structure that enhanced long-term mechanical strength. Finally, the cement provided initial structural support, activated other components, and stimulated the hydration reaction, contributing to the formation of a solid binder. Chemical analysis confirmed that the combination of MSWI-FA, GGBFS, and cement was an optimal choice for stabilizing contaminated industrial soils. This was due to the reactive properties of W-FA, the ability of GGBFS to function as a hydraulic binder, and the immediate strength provided by cement.

Table 2 Chemical composition of MSWI-FA, W-FA and GGBFS. Weight percentage of the main elements identified

Compositions	MSWI-FA	W-FA	GGBFS
Ca	24.31	26.18	32.58
Si	5.83	5.45	30.12
Al	3.32	3.17	12.74
Mg	2.71	2.68	7.92
Fe	2.58	2.51	11.63
Na	1.66	1.23	4.81
Cl	21.20	8.77	–
C	16.35	15.42	–
S	8.57	7.94	–
$CaCO_3$	17.1	16.5	–
$Ca(OH)_2$	13.2	15.5	–
$CaSO_4{\cdot}2H_2O$	6.8	7.1	–
NaCl	3.1	2.9	–
KCl	4.0	3.2	–
SiO_2	9.4	10.3	47.3
C_3S	–	–	11.7
Fe_2O_3	–	–	5.8
MgO	–	–	4.1
$CaAl_2O_4$	–	–	3.6

2.2 Mix design characterization

In the S/S process, selecting the appropriate quantities of each substance is crucial for soil inertization and ensuring environmental safety. This study analyzes three different mixtures of contaminated soil

Table 3 Percentage proportions of the StabSoil mixes considered

	Mix1	Mix2	Mix3
Cement	10	10	10
MSWI-FA	15	10	5
GGBFS	25	20	15
Soil	50	60	70

Table 4 Values of mixes in grams

	Mix1	Mix2	Mix3	Units
Cement	20	20	20	g
MSWI-FA	30	20	10	g
GGBFS	50	40	30	g
Soil	100	120	140	g

and stabilizing materials, with proportions determined based on soil characteristics, the pollutants present, and the individual properties of the stabilization materials used. The objective was to partially replace traditional cement with substances capable of immobilizing contaminants and enhancing durability in a sustainable manner. The proportions used in the mixture were determined after a series of trial mixes, and Table 3 shows the various proportions used in the different mixes and the Table 4 shows the amount in grams. Mix 1 contains the least amount of soil and, therefore, has a higher proportion of GGBFS (partially replacing cement) to enhance the final product's strength. In Mix 2, the soil content increases to 60%, while GGBFS is reduced to 20%. Finally, Mix 3 consists of 70% soil, resulting in the highest density among the three. For the parametric analysis, the specific weight of each sample was determined. Each sample has a mass of 200 g, and after calculating the volume of each mix, the corresponding specific weights were determined and are reported in Table 5. Figure 1 shows three different designs.

3 An analytic study of the bandgap response of metaconcretes

Figure 2 shows the cross-section of a rubber-coated spherical particle of stabilized and solidified soil, forming the aggregate element of a cubic unit cell

Table 5 Volume and specific weights of mixes analyzed

	Mix1	Mix2	Mix3	Units
Volume	160	150	145	cm^3
Specific weight	1250	1330	1380	kg/m^3

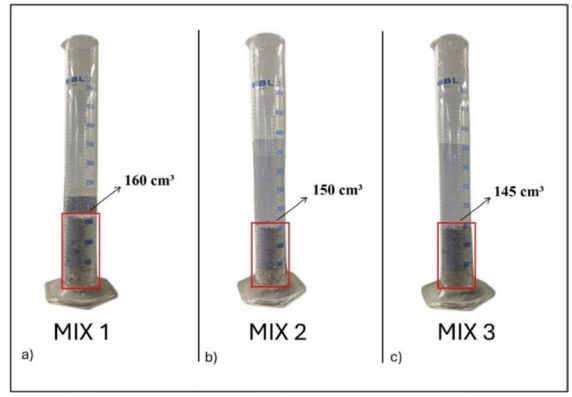


Fig. 1 Photo of the mix design inside the graduated cylinder. **a** Mix 1; **b** Mix 2; **c** Mix 3

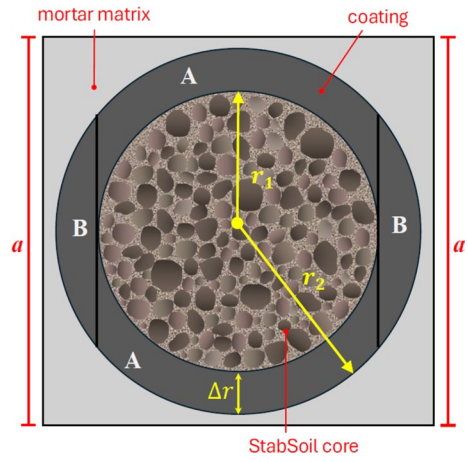


Fig. 2 Illustration of the elements of the SSMC unit cell

with edge length a in an SSMC. The core of the aggregate, which acts as an internal resonator, consists of a spherical particle of a stabilized soil (StabSoil) with radius r_1, or alternatively, a sphere of equivalent mass made from the same material but exhibiting a different shape [30]. The soft coating is made of a natural rubber with density ρ_w of 900 kg/m^3, Young modulus $E_w = 0.01$ GPa and Poisson's

ratio $\upsilon_w = 0.49$ [28, 29]. The coating exhibits external radius r_2 and thickness $\Delta r = r_2 - r_1$ (Fig. 2).

The theory presented in [27] studies the frequency bandgap response of a strip of metaconcrete unit cells forming a rod element (Fig. 3), using a simplified homogenization theory. It predicts that mechanical waves impacting the rod with a frequency f within the *bandgap* interval $[f_1, f_2]$ cannot propagate through the system. The lower frequency f_1 corresponds to the activation of a pure translational vibration motion of the resonator, with the matrix remaining (theoretically) at rest. In contrast, the cutoff frequency f_2 marks the activation of a relative vibration motion between the matrix and the resonator.

According to the theory presented in [27], the bandgap limiting frequencies can be computed using the following equations:

$$f_1 = \frac{1}{2\pi}\sqrt{\frac{k}{m_1}} \tag{1}$$

$$f_2 = \frac{1}{2\pi}\sqrt{\frac{k(m_1+m_2)}{m_1 m_2}} \tag{2}$$

Here, m_1 and m_2 represent the equivalent (homogenized) masses of the resonator and the matrix, respectively, while k is the equivalent stiffness coefficient of the soft coating, computed as follows

$$k = \left[\frac{3\pi}{4}(\lambda_w + 2\mu_w) + \frac{8\pi}{3}\mu_w\right]\frac{(r_1+r_2)^2}{4(r_2-r_1)} \tag{3}$$

λ_w and μ_w being the Lamé constants of the material forming the soft coating. These constants are given by

$$\lambda_w = \frac{\nu_w E_w}{(1+\nu_w)(1-2\nu_w)}, \mu_w = \frac{E_w}{2(1+\nu_w)} \tag{4}$$

In Eq. (4), E_w and ν_w denote the Young modulus and Poisson's ratio of the soft coating material, respectively. Equation (3) assumes that the coating material is subdivided into multiple elements distributed around the resonator, with their stiffness properties suitably combined to determine the overall stiffness constant k (see [27] for more details). Regarding the equivalent masses, the model presented in [27] divides the coating into regions (A) and (B), as shown in Fig. 2. It assumes that region (B) vibrates with the resonator, carrying its mass m_{wB}. The mass m_{wA} of region (A) is instead partially attributed to m_1 and partially to m_2, in such a way that it results in

$$m_1 = m_a + m_{wA}\frac{\alpha}{1+\alpha} \tag{5}$$

$$m_2 = m_c + m_{wB} + m_{wA}\frac{1}{1+\alpha} \tag{6}$$

Here, m_a and m_c denote the mass of the StabSoil resonator and the mass of the matrix in the SSMC unit cell, respectively, while α denotes the coefficient defined through

$$\alpha = \frac{m_{wA} + m_{wB} + m_c}{m_{wA} + m_a} \tag{7}$$

The following expressions for the individual masses appearing in Eqns. (5)–(6) are easily obtained.

$$m_a = \rho_a \frac{4}{3}\pi r_1^3 \tag{8}$$

$$m_c = \rho_c\left(a^3 - \frac{4}{3}\pi r_2^3\right) \tag{9}$$

$$m_{wB} = \rho_w \frac{4}{3}\pi\left(r_2^2 - r_1^2\right)^{\frac{3}{2}} \tag{10}$$

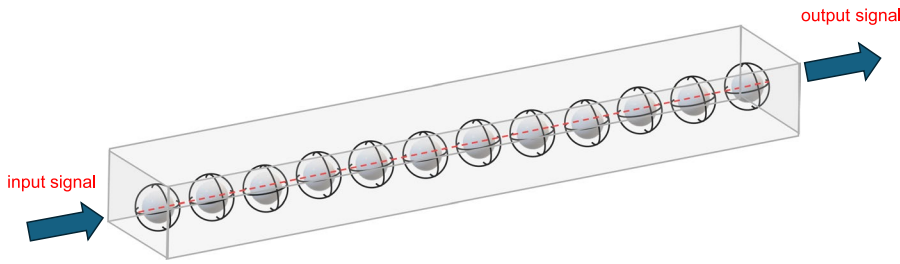


Fig. 3 One-dimensional rod element made of a SSMC

$$m_{wA} = \rho_w \frac{4}{3}\pi\left(r_2^3 - r_1^3\right) - m_{wB} \tag{11}$$

ρ_a, ρ_c and ρ_w respectively denoting the mass densities of the resonator, the matrix, and the soft coating.

4 Parametric study of the bandgap frequencies

We conducted a parametric study on the frequency bandgap response of various rod elements made of SSMC, utilizing the analytical formulation presented in the previous section. We considered the three mix designs illustrated in Sect. 2, along with different geometries of the SSMC unit cell. Our analysis covers four *scenarios*, each corresponding to a different unit cell design, with every design examined for each mix design analyzed.

- *Scenario 1* (hereafter labeled "CS") examines how the bandgap limiting frequencies vary with an increasing core size of the SSMC.
- *Scenario 2* ("CT") investigates the influence of variations in soft coating thickness on these frequencies.
- *Scenario 3* ("CB") analyzes the combined effect of both parameters.
- *Scenario 4* ("*a*") explores the influence of cell length *a* on the bandgap response.

The parametric analysis utilizes the material properties presented in Tables 5 and 6 for the employed mix designs and soft coating, respectively. A lightweight mortar matrix with mass density of 1130 kg/m³ was employed [28]. The analyzed unit cell geometries correspond to the designs illustrated in Table 7, labeled in the format "SSMC-Scenario Label-Design Number ID".

The first three scenarios use a cell size of $a = 35$ mm and assume various values for the radius of the StabSoil core particle (r_1) and the external radius of the soft coating (r_2). In particular, the SSMC-CS cases assume r_1 varies between 10 and 13 mm in increments of 0.5 mm, while r_2 varies between 12 and 15 mm, maintaining a constant coating thickness $\Delta r = r_2 - r_1 = 2$ mm. The SSMC-CT cases keep r_1 constant at 9 mm, while allowing the coating thickness to vary between 0.5 and 5.0 mm. In contrast, the SSMC-CB cases keep r_2 constant at 12 mm, while r_1 varies between 7 and 11.5 mm, thereby altering both the core radius and the soft coating thickness (combined effect). Similar scenarios were examined in [27–29] for different types of metaconcrete. Finally, the SSMC- *a* cases allow the cell size *a* to vary between 35 and 45 mm, while keeping the core radius

Table 6 Physical and mechanical properties of the soft coating

Mass density	Elastic modulus	Poisson's ratio
900 kg/m^3	0.01×10^9 N/m^2	0.49

Table 7 Geometries of the analyzed SSMC unit cells

		a [mm]	r_1[mm]	r_2[mm]
Scenario 1	SSMC-CS1	35	10	12
	SSMC-CS2	35	10.5	12.5
	SSMC-CS3	35	11	13
	SSMC-CS4	35	11.5	13.5
	SSMC-CS5	35	12	14
	SSMC-CS6	35	12.5	14.5
	SSMC-CS7	35	13	15
Scenario 2	SSMC-CT1	35	9	9.5
	SSMC-CT2	35	9	10
	SSMC-CT3	35	9	11
	SSMC-CT4	35	9	12
	SSMC-CT5	35	9	13
	SSMC-CT6	35	9	14
Scenario 3	SSMC-CB1	35	11.5	12
	SSMC-CB2	35	11	12
	SSMC-CB3	35	10	12
	SSMC-CB4	35	9	12
	SSMC-CB5	35	8	12
	SSMC-CB6	35	7	12
Scenario 4	SSMC-*a*1	35	12	10
	SSMC-*a*2	36	12	10
	SSMC-*a*3	37	12	10
	SSMC-*a*4	38	12	10
	SSMC-*a*5	39	12	10
	SSMC-*a*6	40	12	10
	SSMC-*a*7	41	12	10
	SSMC-*a*8	42	12	10
	SSMC-*a*9	43	12	10
	SSMC-*a*10	44	12	10
	SSMC-*a*11	45	12	10

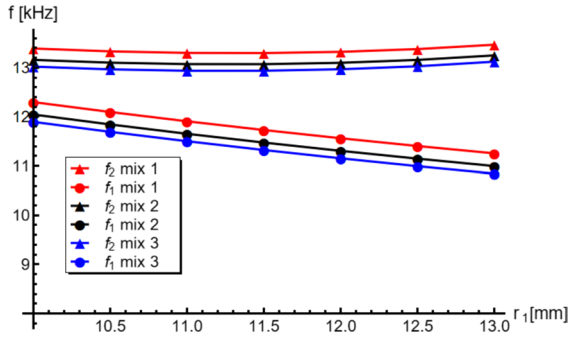


Fig. 4 Scenario 1: Influence of core size on the limiting bandgap frequencies f_1 and f_2

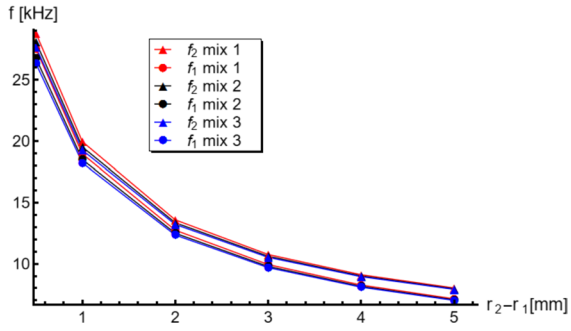


Fig. 5 Scenario 2: Influence of coating thickness on f_1 and f_2

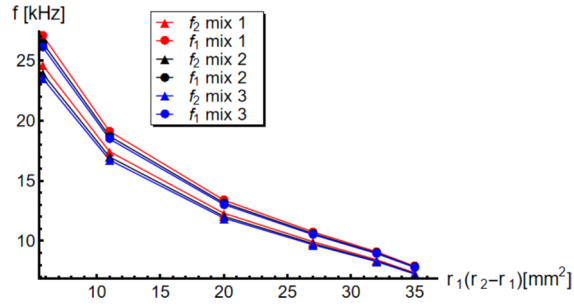


Fig. 6 Scenario 3: Influence of combined geometric parameters on f_1 and f_2

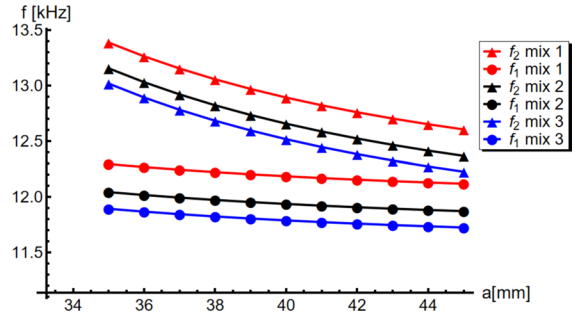


Fig. 7 Scenario 4: Influence of the SSMC cell size a on f_1 and f_2

fixed at 10 mm and the soft coating thickness fixed at 2 mm.

The results shown in Figs. 4, 5 and 6 align with similar findings reported in references [27–29] for different types of metaconcretes. Figure 4 illustrates that the bandgap-limiting frequencies range between 10.8 and 13.5 kHz, with f_2 nearly constant and f_1 slightly decreasing as the size of the SSMC aggregates increases within the analyzed range of r_1, while the thickness of the soft coating remains fixed (Scenario 1). Additionally, the difference $f_2 - f_1$, which represents the bandgap width, increases as r_1 increases under the same SSMC design scenario. An increase in the soft coating thickness, as studied in Scenario 2, as well as the combined change in core radius and soft coating thickness analyzed in Scenario 3, results in a noticeable decrease in the values of both f_2 and f_1 with increasing $\Delta r = r_2 - r_1$ and $r_1 \Delta r$, respectively, as observed in Figs. 5 and 6. These frequencies decrease to approximately 7–8 kHz, starting from a maximum value of 27–29 kHz (f_2), depending on the mix design of the core particles.

Lastly, increasing the overall SSMC cell size while keeping the SSMC aggregate size unchanged (Scenario 4) results in a slight reduction of the bandgap-limiting frequencies, with a more pronounced decrease in the cut-off frequency f_2 (Fig. 7). In all the above design scenarios, we observed limited variations in the bandgap limiting frequencies when modifying the mix design of the examined StabSoil particles. This is because their mass densities, a crucial factor influencing the bandgap frequency, are highly similar. However, we observe a slight decrease in both f_2 and f_1 when transitioning from Mix 1 to Mix 3, due to an increase in the mass density of the StabSoil core particles (cf. Table 5).

5 Concluding remarks

We have introduced a novel type of metaconcrete, labeled SSMC, which incorporates core particles of stabilized and solidified soil to form concrete aggregates encapsulated in a soft material coating (e.g., natural rubber). Various SSMC mix designs were developed, and a detailed parametric analysis was conducted to examine how the bandgap frequency of SSMC varies with the physical and geometric properties of its components [27]. The results indicate that while small variations in core density have a minimal effect on bandgap width, changes in core radius have a more significant influence. Additionally, the study found that as coating thickness and unit cell size increase, the limiting bandgap frequencies decrease. These findings demonstrate that contaminated soils can be safely repurposed for environmental protection and serve as valuable components in civil engineering applications, particularly in blast and seismic-resistant structures [20]. Furthermore, the production of SSMC offers notable environmental benefits, including the remediation of large quantities of contaminated soil and the reuse of waste materials such as municipal solid waste incineration ash.

Several aspects of this study open promising avenues for further research. First, laboratory testing of SSMC core particles is essential to accurately assess their mechanical properties, such as stiffness, strength, and failure mechanisms. These experimental results will be critical for informing and refining numerical simulations of SSMC-based structural elements subjected to blast loading and wave propagation phenomena [27–29], thereby helping to validate the analytical findings presented in this study. A better understanding of the core particle behavior under high strain-rate conditions will also improve the predictive capabilities of the simulation models. Second, experimental testing of SSMC samples under dynamic loading conditions [23–26] is needed to corroborate the trends and sensitivities identified in the parametric analysis. Dynamic experiments will help capture complex material responses, such as strain-rate effects and energy dissipation mechanisms, that are difficult to fully characterize through analytical or numerical methods alone. Such experimental validation will enhance the reliability of the proposed models when applied to real-world scenarios. Additionally, future research will aim to explore a broader range of StabSoil mix designs with increasingly diverse compositions [33], including variations in particle types, cementitious binders, and additive contents. This expanded experimental campaign will not only help optimize material performance for specific applications but also support the development of tailored SSMC formulations with enhanced mechanical and dynamic properties. Overall, the experimental outcomes from these future studies will provide a robust foundation for multiscale mechanical modeling of SSMC cementitious materials, accounting for crack-damage phenomena [34–36] and bridging the gap between microscale particle behavior and macroscale structural performance. A promising direction for future research also involves the use of stabilized soils within seismic metamaterials composed of rubber-coated aggregates. In particular, further investigation is warranted into the seismic wave shielding effects of suitably designed metamaterials incorporating rubber-coated StabSoil inclusions [37].

Acknowledgements The authors gratefully acknowledge the great support received by Gerardo Carpentieri (University of Salerno) in the development of the present work.

Author contributions A.P.: funding acquisition, supervision, investigation, writing—original draft, writing—review and editing; G.D.C.: investigation, methodology, formal analysis, writing—original draft, validation, writing— review and editing; A.A.: data curation, investigation, validation, writing—original draft, writing—review and editing; F.F.: funding acquisition, supervision, methodology, writing—original draft, writing— review and editing; I.F.: investigation, methodology, resources, supervision, writing—original draft, validation, writing— review and editing; All authors have read and agreed to the published version of the manuscript.

Funding Open access funding provided by Università degli Studi di Salerno within the CRUI-CARE Agreement. This work was supported by the National Recovery and Resilience Plan (NRRP), Mission 4, Component 2, Investment 1.1, Call for tender No. 1409 published on 14.9.2022 by the Italian Ministry of University and Research (MUR), funded by the European Union—NextGenerationEU—Project Title 'Stabilization of contaminated soils' (STABSOIL)—P2022 CR8 AJ—CUP D53D23018180001 (A.P. PI). It has also been supported by the National Recovery and Resilience Plan (NRRP), Mission 4, Component 2, Investment 1.1, Call for tender No. 104 published on 2.2.2022 by the Italian Ministry of University and Research (MUR), funded by the European Union—NextGenerationEU—Project Title 'Innovative tensegrity lattices and architectured metamaterials' (ILAM)—20224LBXMZ—CUP D53D23003020006 (F.F. PI). F.F. also acknowledges support by the Italian Ministry of Foreign Affairs and International Cooperation within the Italy-USA Science and Technology Cooperation Program 2023–2025, Project 'Next-generation

green structures for natural disaster-proof buildings', grant number US23GR15. G.D.C. thanks the Italian Dottorato di Interesse Nazionale 'Defense against Natural Risks and Ecological Transition of Built Environment'.

Data availability No datasets were generated or analysed during the current study.

Declarations

Conflict of interest The authors declare no competing interests.

Open Access This article is licensed under a Creative Commons Attribution 4.0 International License, which permits use, sharing, adaptation, distribution and reproduction in any medium or format, as long as you give appropriate credit to the original author(s) and the source, provide a link to the Creative Commons licence, and indicate if changes were made. The images or other third party material in this article are included in the article's Creative Commons licence, unless indicated otherwise in a credit line to the material. If material is not included in the article's Creative Commons licence and your intended use is not permitted by statutory regulation or exceeds the permitted use, you will need to obtain permission directly from the copyright holder. To view a copy of this licence, visit http://creativecommons.org/licenses/by/4.0/.

References

1. Tajudin SAA, Azmi MAM, Nabila ATA (2016) Stabilization/solidification remediation method for contaminated soil: a review. IOP Conf Ser Mater Sci Eng 136:012043
2. Shi C, Spence R (2010) Designing of cement-based formula for solidification/stabilization of hazardous, radioactive, and mixed wastes. Crit Rev Environ Sci Technol July-August 2004:391–417
3. Dermatas D, Meng X (2003) Utilization of fly ash for stabilization/solidification of heavy metal contaminated soils. Eng Geol 70(3):377–394
4. Yin C-Y, Mahmud H, Shaaban M (2006) Stabilization/solidification of lead-contaminated soil using cement and rice husk ash. J Hazard Mater 137:1758–1764
5. Wang H, Zhu Z, Pu S, Song W (2022) Solidification/stabilization of Pb2+ and Cd2+ contaminated soil using fly ash and GGBS based geopolymer. Arab J Sci Eng 47(4):4385–4400
6. Mao Y, Muhammad F, Yu L, Xia M, Huang X, Jiao B, Shiau Y, Li D (2019) The solidification of lead-zinc smelting slag through bentonite supported alkali-activated slag cementitious material. Int J Environ Res Public Health 16(7):1121
7. Juenger MCG, Winnefeld F, Provis JL, Ideker JH (2011) Advances in alternative cementitious binders. Cem Concr Res 41(12):1232–1243
8. Andini S, Cioffi R, Colangelo F, Grieco T, Montagnaro F, Santoro L (2008) Coal fly ash as raw material for the manufacture of geopolymer-based products. Waste Manag 28(2008):416–423
9. Loginova E, Proskurnin M, Brouwers HJH (2019) Municipal solid waste incineration (MSWI) fly ash composition analysis: a case study of combined chelatant-based washing treatment efficiency. J Environ Manag 235:480–488
10. Race M (2017) Applicability of alkaline precipitation for the recovery of EDDS spent solution. J Environ Manag 203:358–363
11. Yang Z, Tian S, Ji R, Liu L, Wang X, Zhang Z (2017) Effect of water-washing on the co-removal of chlorine and heavy metals in air pollution control residue from MSW incineration. Waste Manag 68:221–231
12. Özbay E, Erdemir M, Durmuş Hİ (2016) Utilization and efficiency of ground granulated blast furnace slag on concrete properties–a review. Constr Build Mater 105:423–434
13. Teng S, Lim TYD, SabetDivsholi B (2013) Durability and mechanical properties of high strength concrete incorporating ultra fine ground granulated blast-furnace slag. Constr Build Mater 40:875–881
14. Çakır Ö, Aköz F (2008) Effect of curing conditions on the mortars with and without GGBFS. Constr Build Mater 22:308–314
15. Wang L, Tsang D, Poon CS (2014) Green remediation and recycling of contaminated sediment by waste-incorporated stabilization/solidification. Chemosphere 122:257–264
16. Reza A, Anzum S, Saha RC, Chakraborty S (2018) Implementation of solidification/stabilization process to reduce hazardous 841 impurities and stabilize soil matrices. E3S Web of Conferences.
17. Todaro F, Colangelo F, De Gisi S, Farina I, Ferone C, Labianca C, Petrella A, Cioffi R, Notarnicola M (2023) Recycling of contaminated marine sediment and industrial by-products through combined stabilization/solidification and granulation treatment. Materials 16:2399
18. Couvidat J, Benzaazoua M, Chatain V, Bouamrane A, Bouzahzah H (2016) Feasibility of the reuse of total and processed contaminated marine sediments as fine aggregates in cemented mortars. Constr Build Mater 112:892–902
19. Wang F, Wang H, Al-Tabbaa A (2014) Leachability and heavy metal speciation of 17-year old stabilised/solidified contaminated site soils. J Hazard Mater 278:144–151
20. Mitchell SJ, Pandolfi A, Ortiz M (2014) Metaconcrete: designed aggregates to enhance dynamic performance. J Mech Phys Solids 65:69–81
21. Milton GW, Willis JR (2007) On modifications of Newton's second law and linear continuum elastodynamics. Proc R Soc A Math Phys Eng Sci 463(2079):855–880
22. Mitchell SJ, Pandolfi A, Ortiz M (2015) Investigation of elastic wave transmission in a metaconcrete slab. Mech Mater 91:295–303
23. Briccola D, Ortiz M, Pandolfi A (2017) Experimental validation of metaconcrete blast mitigation properties. J Appl Mech 84(3):031001
24 Briccola D, Tomasin M, Netti T, Pandolfi A (2019) The influence of a lattice-like pattern of inclusions on the attenuation properties of metaconcrete. Front Mater 6:35

25. Briccola D, Cuni M, De Juli A, Ortiz M, Pandolfi A (2021) Experimental validation of the attenuation properties in the sonic range of metaconcrete containing two types of resonant inclusions. Exp Mech 61(3):515–532
26 Briccola D, Pandolfi A (2021) Analysis on the dynamic wave attenuation properties of metaconcrete considering a quasi-random arrangement of inclusions. Front Mater 7:615189
27. Chen J, Zeng X, Umar HA, Xie Y, Long G (2023) Research on vibration reduction performance of metaconcrete based on local resonance theory. J Build Eng 71:106520
28. Xu C, Chen W, Hao H, Jin H (2021) Effect of engineered aggregate configuration and design on stress wave attenuation of metaconcrete rod structure. Int J Solids Struct 232:111182
29. Fireha A, Zhou R, Liu Y, Wang L-G, Wang W, Wang J (2024) Mesoscale modelling of metaconcrete containing rubber aggregates towards wave attenuation against impact loadings. Case Stud Construct Mater 20:e03127
30. Xu C, Chen W, Hao H (2020) The influence of design parameters of engineered aggregate in metaconcrete on bandgap region. J Mech Phys Solids 139:103929
31. Pranno A, Greco F, Leonetti L, Lonetti P, Luciano R, De Maio U (2022) Band gap tuning through microscopic instabilities of compressively loaded lightened nacre-like composite metamaterials. Compos Struct 282:115032
32. De Maio U, Greco F, Luciano R, Sgambitterra G, Pranno A (2023) Microstructural design for elastic wave attenuation in 3D printed nacre-like bioinspired metamaterials lightened with hollow platelets. Mech Res Commun 128:104045
33. Petrillo A, Fraternali F, Acampora A, Di Chiara G, Colangelo F, Farina I (2025) Innovative solidification and stabilization techniques using industrial by-products for soil remediation. Appl Sci 15(7):4002
34. De Maio U, Cendón D, Greco F, Leonetti L, Blasi PN, Planas J (2021) Investigation of concrete cracking phenomena by using cohesive fracture-based techniques: a comparison between an embedded crack model and a refined diffuse interface model. Theoret Appl Fract Mech 115:103062
35. De Maio U, Gaetano D, Greco F, Lonetti P, Pranno A (2023) The damage effect on the dynamic characteristics of FRP-strengthened reinforced concrete structures. Compos Struct 309:116731
36. Feo L, Greco F, Leonetti L, Luciano R (2015) Mixed-mode fracture in lightweight aggregate concrete by using a moving mesh approach within a multiscale framework. Compos Struct 123:88–97
37. Miniaci M, Krushynska A, Bosia F, Pugno NM (2016) Large scale mechanical metamaterials as seismic shields. New J Phys 18(8):083041

Publisher's Note Springer Nature remains neutral with regard to jurisdictional claims in published maps and institutional affiliations.